

# Journal of Materials Chemistry A

Accepted Manuscript



This is an *Accepted Manuscript*, which has been through the Royal Society of Chemistry peer review process and has been accepted for publication.

*Accepted Manuscripts* are published online shortly after acceptance, before technical editing, formatting and proof reading. Using this free service, authors can make their results available to the community, in citable form, before we publish the edited article. We will replace this *Accepted Manuscript* with the edited and formatted *Advance Article* as soon as it is available.

You can find more information about *Accepted Manuscripts* in the [Information for Authors](#).

Please note that technical editing may introduce minor changes to the text and/or graphics, which may alter content. The journal's standard [Terms & Conditions](#) and the [Ethical guidelines](#) still apply. In no event shall the Royal Society of Chemistry be held responsible for any errors or omissions in this *Accepted Manuscript* or any consequences arising from the use of any information it contains.



Journal Name

ARTICLE

## Validation of Green Composite Containing Nanocrystalline Mn<sub>2</sub>O<sub>3</sub> and Biocarbon Derived from Human Hair as a Potential Anode for Lithium-ion Batteries

Received 00th January 20xx,  
Accepted 00th January 20xx

DOI: 10.1039/x0xx00000x

www.rsc.org/

Chandra Sekhar Bongu, Saravanan Karupiah and Kalaiselvi Nallathamby \*

**ABSTRACT** : Mn<sub>2</sub>O<sub>3</sub> nanoparticles, encapsulated with nitrogen and sulfur doped randomly oriented graphene sheet like bio-carbon derived from human hair (HHC) form Mn<sub>2</sub>O<sub>3</sub>/HHC nanocomposite through a cheap, scalable and highly reproducible process. Such a Mn<sub>2</sub>O<sub>3</sub>/HHC nanocomposite anode exhibits excellent electrochemical performance, which is superior than that of the pristine Mn<sub>2</sub>O<sub>3</sub> anode in lithium-ion batteries (LIBs). A study state reversible capacity of 990 mAh g<sup>-1</sup> has been obtained at 50 mA g<sup>-1</sup>, which is about 98 % of the theoretical capacity and the highest ever capacity achieved so far with respect to Mn<sub>2</sub>O<sub>3</sub> based anode material. Mn<sub>2</sub>O<sub>3</sub>/HHC nanocomposite anode delivers capacity in the range of 1250 to 450 mAh g<sup>-1</sup>, when the current density is varied from 100 to 2000 mA g<sup>-1</sup>, highlighting the excellent rate capability and reversibility. The reversible specific capacity value obtained for Mn<sub>2</sub>O<sub>3</sub>/HHC nanocomposite anode is at least three times higher than that of the commercial graphite anode. The impressive electrochemical performance of Mn<sub>2</sub>O<sub>3</sub>/HHC nanocomposite anode results from the multiple synergistic advantages offered by HHC, such as enhancing the electrode conductivity, maintaining the structural integrity upon cycling and mitigating the inherent severe volume change. Our results indicate that the currently synthesized Mn<sub>2</sub>O<sub>3</sub>/HHC nanocomposite anode could be considered as a promising candidate for next generation hybrid energy storage applications. The present work indicates a ray of hope to exploit earth abundant, environment friendly and low cost Mn<sub>2</sub>O<sub>3</sub> based composite anodes for high capacity and high rate lithium-ion battery applications.

### Introduction

Energy storage and conversion play a crucial role in addressing the energy management related issues of the modern society, by way of demonstrating their important capabilities in portable electronics, transportation electronics and utility grid. Over the two decades, lithium-ion batteries (LIBs) have dominated the portable electronics market, due to their high energy density and long cycle life.<sup>1,2</sup> However, the successful integration of LIBs to plug-in hybrid vehicles (PHEVs) with a view to reduce the energy dependence on fossil fuels is still far away, because of certain critical shortcomings such as limited theoretical capacity (372 mAh g<sup>-1</sup>) and poorer cycling performance of the commercial graphite anode.<sup>3,4</sup> Therefore, a pressing need arises to develop alternative anode materials for LIBs, which possess larger reversible capacity, long cycle life, desirable rate capability and environmentally benign nature in order to meet with the requirements of next generation energy storage applications.

Towards this direction, over the years, great efforts have been devoted to investigate upon many transition metal oxides bestowed with inherent high capacity to address the aforesaid need of portable and consumer market based electronic equipments.<sup>5-19</sup> Recently, manganese (Mn) based oxides have drawn special research interest, owing to their high specific capacity, natural abundance and excellent catalytic and electrochemical properties. Among them, Mn<sub>2</sub>O<sub>3</sub> has received greater attention due to the higher theoretical capacity (1018 mAh g<sup>-1</sup>) and higher energy density advantages, apart from its low operating potential (average discharge and charge potentials of 0.5 and 1.2V, respectively) versus Li/Li<sup>+</sup>.<sup>20-30</sup>

In general, the practical use of Mn<sub>2</sub>O<sub>3</sub> is still hindered because of certain critical problems that are associated with the unavoidable volume changes experienced upon cycling and the inferior conductivity, which results in poor cycling performance of the battery.<sup>20,21,28</sup> With a view to alleviate such problems, many efforts have been made that include the synthesis of hollow/micro/nano structures with controlled size, shape and internal structural arrangement and to improve the electrochemical performance of Mn<sub>2</sub>O<sub>3</sub>.<sup>23-25,27-30</sup> However, these synthesis methods involve stringent conditions and essential addition of templates, which largely hampers the practical application of Mn<sub>2</sub>O<sub>3</sub> in LIBs.<sup>23-30</sup> In addition to that, loading of active material with graphene or reduced graphene

<sup>a</sup> Address here.

<sup>b</sup> Address here.

<sup>c</sup> Address here.

† Footnotes relating to the title and/or authors should appear here.

Electronic Supplementary Information (ESI) available: [details of any supplementary information available should be included here]. See DOI: 10.1039/x0xx00000x

oxide (rGO) is yet another approach, wherein the absolute volume change experienced by the nanocomposite material during charging and discharging could be reduced in a significant manner. In other words, the added graphene or rGO increases the conductivity of the nanocomposite and acts as a buffering matrix by offering the required space to admit volume changes and to prevent the pulverization.<sup>7, 31-35</sup> However, the bothering issue associated with graphene or rGO is the involvement of costly synthetic protocols with the addition of toxic reducing/oxidizing reagents, which is against the versatile usage of  $\text{Mn}_2\text{O}_3$  for large scale applications. As a result, it becomes the need of the hour to identify alternative carbon hosts without complicating and compromising the properties of the pristine host material. It is worthy in this context to recall our previous work, wherein we have synthesized dual hetero atom doped porous carbon (HHC) from filthy human hair and exploited the as-received HHC as an anode for LIBs.<sup>36</sup> Thanks to the unique arrangement of randomly oriented graphene sheet like structure of HHC, which motivates us further to think about replacing of costly carbon varieties such as graphene and rGO in preparing the metal oxide nanocomposites.

The work thus involves the simple addition of in-house made dual hetero atom containing graphene sheet like porous carbon (HHC) to the pristine  $\text{Mn}_2\text{O}_3$ , wherein HHC acts as an additive to prepare the composite of nanocrystalline  $\text{Mn}_2\text{O}_3$ . Further, the work was initiated with a view to understand whether and to what extent HHC by itself can serve as a compositing host material to mitigate the volume changes of metal oxide anode, especially during cycling process. Particularly, the following attracting features of HHC motivated us to exploit it further as an additive to form the composite of  $\text{Mn}_2\text{O}_3$  and to validate the  $\text{Mn}_2\text{O}_3$ /HHC as a potential anode candidate.

- I. HHC possesses randomly oriented porous graphene sheet like structure, which is expected to eventually provide cushioning effect to address the volume changes and the related stress developed during prolonged cycling process. In addition to that, porous nature of HHC will be advantageous in facilitating easy electrolyte access, thereby reducing the lithium-ion diffusion path in  $\text{Mn}_2\text{O}_3$  and conversion mechanism.
- II. The inferior conductivity of as-prepared  $\text{Mn}_2\text{O}_3$  ( $0.025 \mu\text{S m}^{-1}$ ) will be effectively addressed and improved significantly by the addition of HHC, owing to its excellent electronic conductivity ( $48.5 \text{ S m}^{-1}$ ). As a result,  $\text{Mn}_2\text{O}_3$ /HHC composite anode will perform better even under high rate conditions by allowing the access of fast electron transfer with the help of HHC.
- III. Presence of dual heteroatom may increase the available active sites and effectively modulate the electronic and chemical character of carbon matrix.
- IV. Abundant availability of wasteful human hair has been converted in to value added composite

component using a simple synthesis method, thus offering a possible chance to replace the addition of costly host materials and leading to practical viability for commercialization. Being a sustainable waste and with the conversion of filthy human hair for improving the electrochemical behavior of LIBs we reap the benefits of creating a cleaner environment, which by itself justifies its relevance to energy management related protocols.

It is believed that the multiple synergistic effects of the above mentioned appealing features of HHC will boost the electrochemical performance of pristine  $\text{Mn}_2\text{O}_3$ , especially when used as a composite additive and with the same perception, the current work was undertaken.

In this work, we report on the electrochemical behavior of human hair derived N and S enriched porous graphene sheet like carbon encapsulated  $\text{Mn}_2\text{O}_3$  nanoparticles as one of the newer formulation of composite anodes with appreciable electrochemical behavior in LIBs. Firstly, we have synthesized the  $\text{Mn}_2\text{O}_3$  microcubes that contain symmetrically packed nanoflakes and the flakes are formed out of irregularly shaped nanoparticles obtained from a simple co-precipitation technique.<sup>37</sup> Sonication of such  $\text{Mn}_2\text{O}_3$  microcubes with HHC leads to the dispersion of nanoparticles followed by a low temperature treatment. This is a vulcanizing process, wherein we get nanocrystalline  $\text{Mn}_2\text{O}_3$ , finely dispersed over the chosen carbon matrix. For comparison purpose, we have investigated the electrochemical performance of pristine  $\text{Mn}_2\text{O}_3$  anode also. As expected, the combination of HHC with nanocrystalline  $\text{Mn}_2\text{O}_3$  exhibits high lithium-ion storage capacity and impressive rate capability, owing to the nano sized  $\text{Mn}_2\text{O}_3$  particles and the unique properties of HHC that include improved electronic conductivity, fast lithium-ion storage along with the action of buffering matrix to reduce the severe volume expansion of pristine  $\text{Mn}_2\text{O}_3$  anode during cycling process. In addition, we obtained the highest ever reported reversible lithium storage capacity ( $990 \text{ mAh g}^{-1}$ ) for the currently prepared  $\text{Mn}_2\text{O}_3$ /HHC composite anode, which is far superior than any other  $\text{Mn}_2\text{O}_3$  based anode material.

## Experimental section

### Materials

We have synthesized  $\text{Mn}_2\text{O}_3$  microcubes containing symmetrically packed nanoflakes, wherein the flakes are formed out of irregularly shaped nanoparticles obtained from a simple co-precipitation technique.<sup>37</sup> To prepare the composite of  $\text{Mn}_2\text{O}_3$ , human hair derived carbon (HHC) containing N and S as heteroatoms has been used. To obtain HHC, human hair was collected from a healthy volunteer of our research group. To ensure the quality and consistency, hair was collected from the same person every time.

### Preparation of $\text{Mn}_2\text{O}_3$ /HHC nanocomposite

$\text{Mn}_2\text{O}_3$ /HHC nanocomposite was prepared by mixing the as-received  $\text{Mn}_2\text{O}_3$  microcubes collected from the aforesaid

method, with human hair derived carbon (10 wt%) in water and sonicated for 60 minutes. Such a sonication will lead to the disintegration of microcubes in to nanoparticles and thus paves way to get a homogenous mixing of  $\text{Mn}_2\text{O}_3$  nanoparticles with those of HHC. Subsequently, the contents were heated in the furnace at 400 °C for 2h in Ar atmosphere to get better wrapping of  $\text{Mn}_2\text{O}_3$  with due adherence by added HHC powder. The resulting material is denoted as  $\text{Mn}_2\text{O}_3/\text{HHC}$  nanocomposite. Nanocrystalline  $\text{Mn}_2\text{O}_3$  obtained through sonication of  $\text{Mn}_2\text{O}_3$  microcubes has been considered for physical and electrochemical characterization to compare the performance characteristics of newly formed  $\text{Mn}_2\text{O}_3/\text{HHC}$  composite.

### Physicochemical characterization

The crystal structure information of the synthesized compound was derived from the XRD pattern recorded using Bruker D8 Advance X-ray diffractometer using Ni-filtered  $\text{Cu K}\alpha$  radiation ( $\lambda=1.5406 \text{ \AA}$ ). To study the particle size, surface morphology and the presence of carbon coating, scanning electron microscopy (SEM, JEOL JSM6480LV system), transmission electron microscopy (TEM, Tecnai 20 G2 (FEI make)) and high resolution transmission electron microscopy (HRTEM) were used. The chemical composition of the products has been obtained from X-ray photoelectron spectroscopy (XPS, MULTILAB 2000 Base system with X-ray, Auger and ISS attachments). The surface area and the pore size of the samples were determined by Brunauer–Emmett–Teller (BET) method by nitrogen adsorption/desorption using Quantachrome, NOVA version 11.02.

### Electrochemical Characterization

VMP3 multichannel potentiostat–galvanostat system (Biologic Science Instrument) was used to study the cyclic voltammetry (CV) in the potential window of 0.01–3.0 V and at a scan rate of  $0.1 \text{ mV s}^{-1}$ . Charge–discharge cycling studies were carried out using Arbin cyler. Electrochemical impedance (EIS) measurements were done on a Biologic VMP3 multichannel Potentiostat. The Nyquist plots were recorded potentiostatically by applying an AC voltage of 5 mV amplitude in the 10 kHz to 100 mHz frequency range.

### Electrode fabrication

The anode electrode was fabricated from a mixture of pristine  $\text{Mn}_2\text{O}_3$  or  $\text{Mn}_2\text{O}_3/\text{HHC}$  powder (active material), super P carbon black (additive) and polyvinylidene fluoride (binder) in the weight ratio 80:10:10. The mixture was ground and mixed with N-Methyl pyrrolidin-2-one to form a slurry. The resultant slurry was coated on a thin copper foil and dried at 80 °C, followed by 120 °C for 2 h. Celgard was used as the separator and the electrolyte was 1 M  $\text{LiPF}_6$  dissolved in 1:1 (v/v) mixture of ethylene carbonate (EC)/dimethyl carbonate (DMC). 2032 coin cells were assembled in an Argon-filled glove box and crimp sealed, wherein lithium metal has been used as counter and reference electrode.

## Results and Discussion

### Physicochemical characterization

Fig. 1 shows the XRD pattern of pristine  $\text{Mn}_2\text{O}_3$  and  $\text{Mn}_2\text{O}_3/\text{HHC}$  nano composite. All the diffraction peaks can be exactly indexed to cubic  $\text{Mn}_2\text{O}_3$  (JCPDS card no. 01-1061).<sup>37</sup> There is no difference in the peak pattern and intensity of  $\text{Mn}_2\text{O}_3/\text{HHC}$  composite, which is quite interesting. Further, Raman spectrum of  $\text{Mn}_2\text{O}_3/\text{HHC}$  composite is shown in Fig. S1. Two peaks obtained at  $1320$  and  $1590 \text{ cm}^{-1}$  correspond to the D (defect band, corresponding to the  $\text{A}_1\text{g}$  mode) and G (graphite band, corresponding to the  $\text{E}_2\text{g}$  hexagonal graphitic lattice) band respectively, thus confirming the presence of HHC in  $\text{Mn}_2\text{O}_3/\text{HHC}$  composite. In addition, the observed high intensity peak at  $658$  and the low intensity peaks at  $580$  and  $478 \text{ cm}^{-1}$  evidence the presence of  $\text{Mn}_2\text{O}_3$ , possessing well defined electronic states.<sup>37</sup>

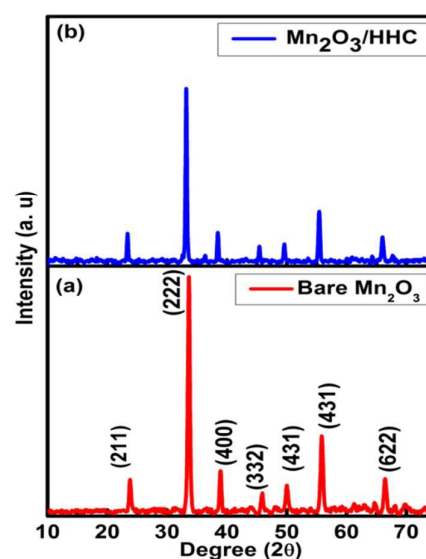


Fig. 1 XRD pattern of (a) nanocrystalline  $\text{Mn}_2\text{O}_3$  and (b) composite with HHC

In order to validate the concentration of HHC present in the  $\text{Mn}_2\text{O}_3/\text{HHC}$  composite, TGA results are furnished in Fig. S2. An approximate weight loss of 8.8 wt% has been noticed around 100–700 °C that corresponds to the removal of HHC from  $\text{Mn}_2\text{O}_3/\text{HHC}$  composite. In other words, the carbon content present in  $\text{Mn}_2\text{O}_3/\text{HHC}$  composite is derived as 8.8 wt % even after annealing process, which is in closer agreement with the externally added 10 wt % of carbon in the form of HHC.

Based on the fascinating properties of HHC,<sup>36</sup> the current study has been designed primarily to investigate the electrochemical properties of the newly formed  $\text{Mn}_2\text{O}_3/\text{HHC}$  nanocomposite and to compare the performance of the same with that of nanocrystalline  $\text{Mn}_2\text{O}_3$  anode with a view to understand the effect of HHC as a composite additive in improving the lithium storage capability under different cycling conditions.

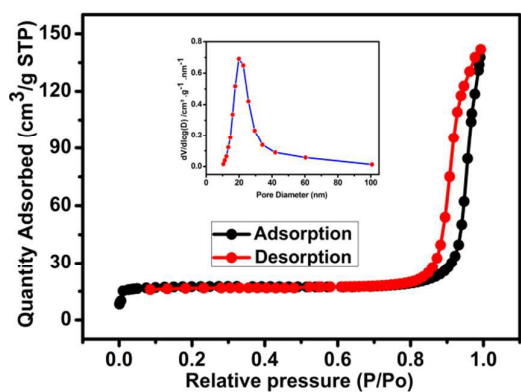


Fig. 2  $N_2$  adsorption-desorption isotherm of  $Mn_2O_3$ /HHC nanocomposite

To determine the surface area and porosity of  $Mn_2O_3$ /HHC,  $N_2$  adsorption isotherm has been recorded. Fig. 2 shows the  $N_2$  adsorption-desorption isotherm of  $Mn_2O_3$ /HHC nano composite. It clearly evidences the type-IV hysteresis loops and the specific surface area is calculated to be  $55.91 \text{ m}^2/\text{g}$ , according to BET method. The pore size distribution curve lies well within the range of 10-100 nm and indicates the presence of meso and macro pores in  $Mn_2O_3$ /HHC composite (Inset).<sup>20,21</sup> Further, the high surface area of  $Mn_2O_3$ /HHC nano composite is expected to offer the formation of most sought after electrode/electrolyte interface for ion accumulation. Similarly, the presence of meso and macro pores in  $Mn_2O_3$ /HHC composite is believed to be beneficial for high rate performance by facilitating rapid lithium-ion diffusion, which in turn may be responsible for an enhanced electrochemical performance.<sup>20</sup>

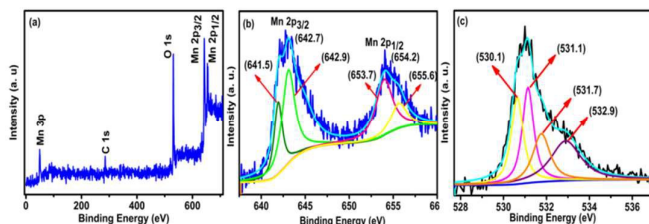


Fig. 3 XPS spectra of  $Mn_2O_3$ /HHC nanocomposite (a) Survey spectrum, (b) Mn 2p and (c) O 1s spectrum

X-ray photoelectron spectroscopy (XPS) is employed to analyze the surface chemical composition and the valence state of nanocrystalline  $Mn_2O_3$  sample and the corresponding  $Mn_2O_3$ /HHC nano composite (Fig. S3 and Fig. 3). In the survey spectrum of  $Mn_2O_3$ /HHC composite, four signals observed at 285.7, 533.3, 643.7 and 656.2 eV are attributed to the characteristic peaks of C1s, O1s, Mn  $2p_{3/2}$  and Mn  $2p_{1/2}$  elements, respectively.<sup>21,37</sup> The deconvoluted spectra of Mn 2p could be seen in Fig. 3b, wherein binding energy values of Mn $2p_{3/2}$  and Mn  $2p_{1/2}$  are observed at approximately 642.7 and 654.2 eV, respectively. The splitting energy difference between Mn  $2p_{3/2}$  and Mn  $2p_{1/2}$  core levels is 11.5 eV,

indicating the presence of  $Mn^{3+}$  in pristine  $Mn_2O_3$  and  $Mn_2O_3$ /HHC nanocomposite. The peak of O1s is centered at 530.2 eV, which is attributed to the presence of  $O^{2-}$ , forming the desired oxide with manganese (Mn). Fig. 3c represents the deconvoluted spectrum of O1s, wherein four peaks located at 530.1, 531.1, 531.7 and 532.9 eV are observed, which may be attributed to the presence of oxygen in the binary oxide.<sup>21,25,37</sup> The high intensity peak for C1s is observed at 284.7 eV in the  $Mn_2O_3$ /HHC nanocomposite survey spectrum (Fig. 3a), which clearly evidences the successful incorporation HHC as a composite additive. Interestingly, such a peak for C1s is found to be absent in the pristine  $Mn_2O_3$  survey spectrum (Fig. S3) which is noteworthy. For clarity, we have reproduced the XPS spectra of HHC in Fig. S4, which in turn substantiates the chemical composition and the presence of heteroatoms, viz. N and S in HHC sample. From the above results, it is clearly evident that the purity of nanocrystalline  $Mn_2O_3$  and the successful incorporation of dual hetero atom doped HHC as additive are confirmed.<sup>36</sup>

Fig. S5 shows the typical scanning electron microscopy (SEM) images of  $Mn_2O_3$ /HHC nano composite. Quite similar to the pristine  $Mn_2O_3$  that contains irregularly shaped nano particles found in the size range of 30-50 nm,  $Mn_2O_3$ /HHC nanocomposite also shows the presence of irregularly shaped  $Mn_2O_3$  nano particles (30-50) and clusters distributed on the porous and graphene sheet like structure of HHC. Such cluster formation is most apparently due to the postvulcanizing treatment induced aggregations of HHC sheets.<sup>38</sup>

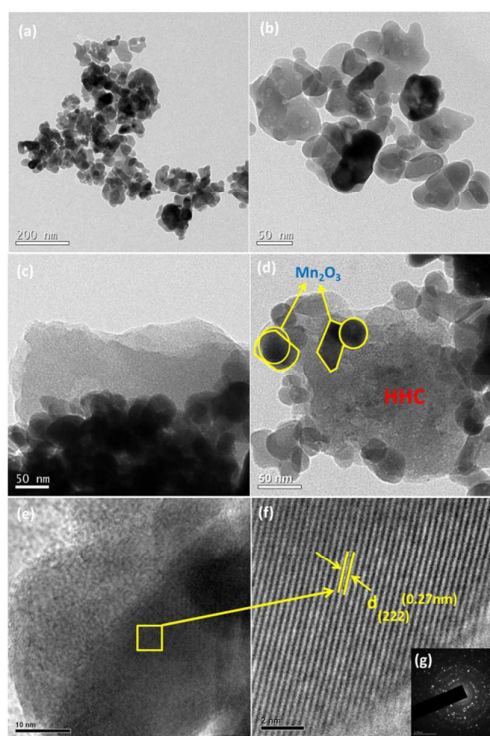


Fig. 4 TEM images of (a-b) nanocrystalline  $Mn_2O_3$ , (c-d)  $Mn_2O_3$ /HHC nanocomposite, (e-f) HRTEM images and (g) SEAD pattern of  $Mn_2O_3$ /HHC nanocomposite

In order to further investigate the internal architecture of  $\text{Mn}_2\text{O}_3/\text{HHC}$  nano composite, transmission electron microscopy (TEM) and high resolution transmission electron microscopy (HRTEM) were deployed. Presence of  $\text{Mn}_2\text{O}_3$  nanoparticles in the size range of 30-50 nm in pristine  $\text{Mn}_2\text{O}_3$  is evident from Fig. 4a and b, which is in good agreement with the SEM images. Further, one can see the uniform distribution of  $\text{Mn}_2\text{O}_3$  nano particles and clusters over the layers of HHC (Fig. 4c and d). It is very interesting that the HHC sheets trap and position multiple  $\text{Mn}_2\text{O}_3$  nano particles in one sheet like peas in a pod rather than forming conformal layers on individual particles (Fig. S6). This add-on advantage on morphological features ensures the effective electronic conductivity of individual  $\text{Mn}_2\text{O}_3$  nano particles.<sup>27</sup> Further, the complete wrapping of nanocrystalline  $\text{Mn}_2\text{O}_3$  particles by HHC sheets plays a key role in mitigating the huge volume changes associated possibly with the individual particles upon during charging and discharging by way of offering a spare space.<sup>7,31-35,38</sup> The HRTEM image of a single particle shows a clear confinement with amorphous carbon (HHC), which is more favorable for conversion reaction (Fig. 4e). It also displays the presence of clear lattice fringes with a d-spacing value of 0.27 nm, which is attributed to the (222) lattice plane of cubic  $\text{Mn}_2\text{O}_3$  and the same is in agreement with the calculated XRD value (Fig. 4f). The SEAD pattern of  $\text{Mn}_2\text{O}_3/\text{HHC}$  nanocomposite, given as inset of Fig. 4g indicates the polycrystalline nature of irregular nanoparticles.

### Electrochemical evaluation

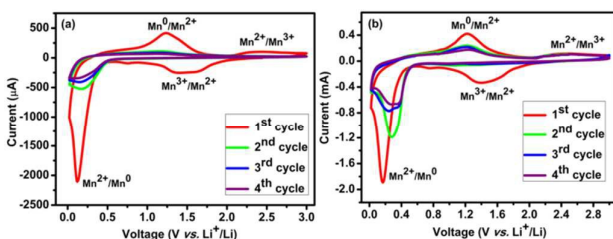


Fig. 5 Cyclic voltammogram of (a) pristine  $\text{Mn}_2\text{O}_3$  and (b)  $\text{Mn}_2\text{O}_3/\text{HHC}$  nanocomposite anode recorded at a scan rate of  $0.1 \text{ mV s}^{-1}$  in the range of 0.01-3.0 V versus  $\text{Li}^+/\text{Li}$

To demonstrate the effect of newly introduced HHC as a composite additive to  $\text{Mn}_2\text{O}_3$  in improving the lithium storage performance, we have investigated and compared the electrochemical properties of pristine  $\text{Mn}_2\text{O}_3$  and  $\text{Mn}_2\text{O}_3/\text{HHC}$  nano structures individually as anode material for LIBs. In particular, cyclic voltammetry (CV) was recorded in the voltage range of 0.01-3.0 V versus  $\text{Li}^+/\text{Li}$  at a scan rate of  $0.1 \text{ mV s}^{-1}$ , with a view to monitor the redox reactions taking place in pristine  $\text{Mn}_2\text{O}_3$  and  $\text{Mn}_2\text{O}_3/\text{HHC}$  nano composite anodes and the results are shown in Fig. 5a and b. The CV curve for the first cycle is substantially different from those of the subsequent cycles, which is not unusual. During the first cathodic process, three main peaks are found at 1.25, 0.75 and

0.2 V. Among them, peaks located at 1.25 and 0.2 V could be attributed to the reduction of  $\text{Mn}^{3+}$  to  $\text{Mn}^{2+}$  and  $\text{Mn}^{2+}$  to  $\text{Mn}^0$  respectively. The peak at 0.75 V is ascribed to the irreversible decomposition of the solvent in the electrolyte to form solid electrolyte interface (SEI).<sup>21,25,37</sup> In the anodic process, there are two oxidation peaks observed at 1.25 and 2.32 V, which are presumably ascribed to the oxidation of  $\text{Mn}^0$  to  $\text{Mn}^{2+}$  and  $\text{Mn}^{2+}$  to  $\text{Mn}^{3+}$ , respectively.<sup>37</sup> In the subsequent cycles, the main cathodic peak is found to get shifted to 0.26 V, which is associated with the reduction of  $\text{Mn}^{3+}$  to  $\text{Mn}^0$ . Compared with the first discharge process, the peak current density and the integrated area of the second cycle are found to get decreased, which is associated with the irreversible capacity loss involved in the process.<sup>21</sup> Interestingly, the integrated area of the CV curves are almost quite similar after the second cycle, which indicates the excellent reversibility of the  $\text{Mn}_2\text{O}_3$  and  $\text{Mn}_2\text{O}_3/\text{HHC}$  anodes upon extended cycling.

Even though both the anodes are basically constructed by nanocrystalline  $\text{Mn}_2\text{O}_3$  particles, which is a desirable property to reduce the transport length of the lithium-ions,  $\text{Mn}_2\text{O}_3/\text{HHC}$  nano composite exhibits better CV behavior in terms of peak current density and larger area compared with that of pristine  $\text{Mn}_2\text{O}_3$  anode, owing to the excellent electronic conductivity offered by HHC.

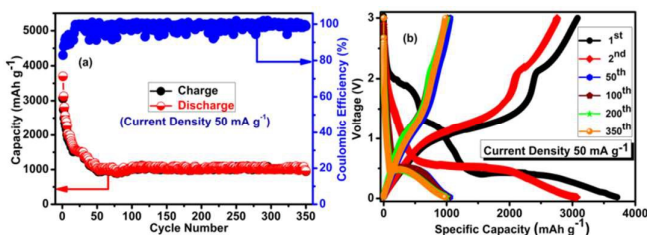


Fig. 6 (a) Cycling performance along with coulombic efficiency and (b) Discharge-charge profile of  $\text{Mn}_2\text{O}_3/\text{HHC}$  nanocomposite anode at a current density of  $50 \text{ mA g}^{-1}$  in the voltage range of 0.01-3.00 V versus  $\text{Li}^+/\text{Li}$ .

The cycling performance of the pristine  $\text{Mn}_2\text{O}_3$  and  $\text{Mn}_2\text{O}_3/\text{HHC}$  nanocomposite anodes at a current density of  $50 \text{ mA g}^{-1}$  is displayed in Fig. S7 and Fig. 6. For the nanocrystalline pristine  $\text{Mn}_2\text{O}_3$  anode, the first cycle discharge and charge capacities are 1500 and 1000  $\text{mAh g}^{-1}$  respectively, and the coulombic efficiency is 66 % (Fig. S7). Likewise, the first cycle discharge and charge capacities of  $\text{Mn}_2\text{O}_3/\text{HHC}$  nanocomposite anode are 3710 and 3070  $\text{mAh g}^{-1}$ , respectively, and the corresponding coulombic efficiency is 83 % (Fig. 6a). In line with this encouraging observation, the irreversible capacity has also been reduced substantially, thus demonstrating the salient advantages of exploitation of HHC as a composite additive. Since the theoretical capacity of  $\text{Mn}_2\text{O}_3$  is  $1018 \text{ mAh g}^{-1}$ , the currently observed excess capacity could be associated with the decomposition of electrolyte at low voltages, generating a SEI layer and the subsequent storage of lithium by interfacial charging at the metal/ $\text{Li}_2\text{O}$  interface.<sup>21,25-30,37</sup> In the second cycle, the discharge capacity of pristine  $\text{Mn}_2\text{O}_3$  is

1010 mAh g<sup>-1</sup> and the charge capacity is 750 mAh g<sup>-1</sup>, corresponding to a coulombic efficiency of 74%. Hereagain, the second cycle discharge and charge capacity values of Mn<sub>2</sub>O<sub>3</sub>/HHC nanocomposite anode are 3070 and 2760 mAh g<sup>-1</sup> respectively, and the coulombic efficiency is 88 %. Hence, it is understood that Mn<sub>2</sub>O<sub>3</sub>/HHC nanocomposite anode, especially due to the presence of externally added HHC to form the composite is playing a significant role in improving the charge-discharge behavior of LIBs. The same has been further substantiated by the inferior extended cycling behavior of pristine Mn<sub>2</sub>O<sub>3</sub> and the superior behavior of Mn<sub>2</sub>O<sub>3</sub>/HHC nanocomposite anode. i.e, Pristine Mn<sub>2</sub>O<sub>3</sub> anode shows a gradual decrease in capacity value during prolonged cycling and delivers a comparatively inferior reversible capacity value of less than 300 mAh g<sup>-1</sup>, especially after 10 cycles. This observation could be correlated to the inferior conductivity of pristine Mn<sub>2</sub>O<sub>3</sub> anode (0.025 μS m<sup>-1</sup>) and the huge volume changes experienced by pristine Mn<sub>2</sub>O<sub>3</sub> anode upon continuous cycling.<sup>31-35</sup> In contrast, Mn<sub>2</sub>O<sub>3</sub>/HHC nanocomposite anode shows a high reversible capacity of 990 mAh g<sup>-1</sup>, even after 350 cycles, with a coulombic efficiency of 99 %. Interestingly, the coulombic efficiency rapidly rises to 99 % from an initial coulombic efficiency of 83%. It is worth mentioning here that the currently investigated Mn<sub>2</sub>O<sub>3</sub>/HHC nanocomposite anode delivers 98 % of the theoretical capacity of Mn<sub>2</sub>O<sub>3</sub> (1018 mAh g<sup>-1</sup>), which is 3 times higher when compared with the theoretical capacity of graphite (372 mAh g<sup>-1</sup>). To our knowledge, this is the maximum value achieved so far with regard to Mn<sub>2</sub>O<sub>3</sub> anode material reported in the literature (Table 1).<sup>20-30</sup>

As already mentioned in the introduction part, the complete wrapping of nanocrystalline Mn<sub>2</sub>O<sub>3</sub> with the hierarchically arranged porous and sheet like structure of HHC offers a conducting network between the nano particles, which in turn accommodates the severe volume changes experienced by nanocrystalline Mn<sub>2</sub>O<sub>3</sub> during cycling process. As a result, a favorable charge transfer reaction has been facilitated exclusively by the added HHC in the Mn<sub>2</sub>O<sub>3</sub>/HHC nanocomposite anode. In addition, HHC containing hetero atoms with defects that are chemically active can further increase the electrical conductivity and improve the Li<sup>+</sup> storage ability of Mn<sub>2</sub>O<sub>3</sub>/HHC nanocomposite anode.<sup>36,38,39</sup> More interestingly, the simple strategy of exploiting HHC as a composite additive is found to be advantageous in improving the electrochemical performance of the pristine Mn<sub>2</sub>O<sub>3</sub> to the extent that Mn<sub>2</sub>O<sub>3</sub>/HHC anode of the present study is exhibiting superior properties over a wide variety of Mn<sub>2</sub>O<sub>3</sub> based anode materials reported in the literature (Table 1).<sup>20-30</sup> From the table, it is apparently seen that Mn<sub>2</sub>O<sub>3</sub>, prepared by various research groups with great care to obtain different size, shape, morphology, internal structure and porosity apart from the effect of introducing a dopant exhibit lesser capacity values under the influence of varying current density in range of 50- 2000 mA g<sup>-1</sup>, especially when compared with the performance of Mn<sub>2</sub>O<sub>3</sub>/HHC nanocomposite anode of the current study.

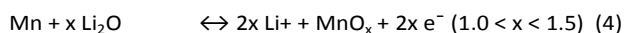
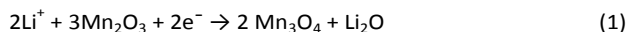
In other words, this table clearly evidences the superiority of currently examined Mn<sub>2</sub>O<sub>3</sub>/HHC anode and the relatively higher capacity values observed with the Mn<sub>2</sub>O<sub>3</sub>/HHC anode with that of the corresponding pristine Mn<sub>2</sub>O<sub>3</sub> anode and demonstrates the significantly improved electrochemical properties due to the exploration of HHC as a composite additive for Mn<sub>2</sub>O<sub>3</sub> anode.

**Table 1** Comparison of specific capacity values of currently observed and reported category Mn<sub>2</sub>O<sub>3</sub> anodes investigated under the influence of various current density conditions to understand the superiority of present work.

Material	Capacity Observed at Current Density (mA g <sup>-1</sup> ) Conditions							Ref. No
	50	100	200	400	800	1000	2000	
<b>Mn<sub>2</sub>O<sub>3</sub>/HHC nanocomposite</b>	<b>1415</b>	<b>1250</b>	<b>1060</b>	<b>890</b>	<b>760</b>	<b>600</b>	<b>440</b>	<b>Present Work</b>
Mn <sub>2</sub> O <sub>3</sub> Hollow Cubes	-	800	620	-	-	410	350	20
Cu-Doped Mn <sub>2</sub> O <sub>3</sub>	-	756	561	431	303	-	-	21
Mn <sub>2</sub> O <sub>3</sub> Sheet-like structure	850	700	610	-	-	-	-	22
Double-shelled Mn <sub>2</sub> O <sub>3</sub>	-	-	900	790	720	-	-	23
Mn <sub>2</sub> O <sub>3</sub> Hollow Spheres	-	-	890	791	650	-	-	23
Porous Mn <sub>2</sub> O <sub>3</sub> microspheres	-	900	-	-	-	-	-	24
Mn <sub>2</sub> O <sub>3</sub> Microspheres	-	913	451	-	-	138	-	25
Mn <sub>2</sub> O <sub>3</sub> Nanocoons	900	650	500	380	-	-	-	26
Mn <sub>2</sub> O <sub>3</sub> Straw-sheaf-shaped	-	550	440	370	270	-	-	27
Porous hierarchical Mn <sub>2</sub> O <sub>3</sub> hollow microspheres	-	751	-	611	511	-	-	28
Mn <sub>2</sub> O <sub>3</sub> Nanoplates	-	1000	840	750	-	590	380	29
Mn <sub>2</sub> O <sub>3</sub> Microspheres assembled porous nanosheets	-	1190	908	677	508	-	-	30
Mn <sub>2</sub> O <sub>3</sub> Microcubes/CRC	525	457	335	183	-	-	-	37

Fig. 6b illustrates the 1<sup>st</sup>, 2<sup>nd</sup>, 50<sup>th</sup>, 100<sup>th</sup>, 200<sup>th</sup> and 350<sup>th</sup> charge-discharge voltage profile of Mn<sub>2</sub>O<sub>3</sub>/HHC nano composite anode in the voltage range of 0.01-3.0 V vs. Li<sup>+</sup>/Li at a current density of 50 mA g<sup>-1</sup>. The first discharge curve shows three distinct plateaus, as seen in Fig. 6b. The initial drop in voltage from 3.0 to 1.35 V and 1.35 to 0.34 V could be attributed to the reduction of Mn<sup>3+</sup> to Mn<sup>2+</sup>, caused by the lithium insertion reaction.<sup>21</sup> In other words, the aforesaid voltage drop could be associated with the formation of Mn<sub>3</sub>O<sub>4</sub> from Mn<sub>2</sub>O<sub>3</sub> (1.35 V) and MnO from Mn<sub>3</sub>O<sub>4</sub> (0.34 V). Subsequently, a voltage drop from 0.34 to 0.01 V is seen, which could be related to the reduction of Mn<sup>2+</sup> to Mn<sup>0</sup>.<sup>25</sup> In short, the new plateau at 0.2 V could be ascribed to the phase transformation reaction including the reduction of MnO to Mn<sup>0</sup> and the formation of Li<sub>2</sub>O.<sup>30,37</sup> In the charge profile, the wide slope existing between 1.2 to 2.2 V could be associated with the oxidation of Mn<sup>0</sup> to Mn<sup>2+</sup> and Mn<sup>2+</sup> to Mn<sup>3+</sup>. In other words, the plateau at 1.2 V may be related to the formation of MnO from Mn<sup>0</sup> and the plateau at 2.2 V corresponds to the reaction between Li<sub>2</sub>O and MnO, leading to the formation of

MnO and MnO<sub>x</sub> mixtures.<sup>37</sup> Probable reactions involved in this charge-discharge process are shown below.



Surprisingly, the Mn<sub>2</sub>O<sub>3</sub>/HHC nanocomposite anode shows a well-defined, flat and stable plateau even after 350 cycles, which in turn confirms the beneficial role of HHC in increasing the excellent reversibility of the above mentioned electrochemical reactions involved in Mn<sub>2</sub>O<sub>3</sub>/HHC nanocomposite anode. On the other hand, the pristine Mn<sub>2</sub>O<sub>3</sub> shows poor reversibility (rapid capacity decay), due to the inferior conductivity and huge volume change that occurs during cycling, which leads to irreversible electrochemical reactions.<sup>31-35,37</sup>

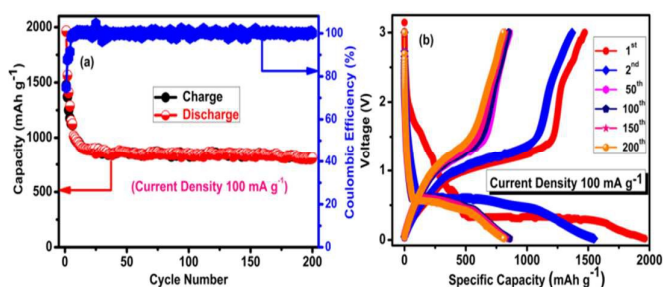


Fig. 7 (a) Cycling performance along with coulombic efficiency and (b) Discharge-charge profile of Mn<sub>2</sub>O<sub>3</sub>/HHC nanocomposite anode at a current density of 100 mA g<sup>-1</sup> in the voltage range of 0.01-3.00 V versus Li<sup>+</sup>/Li.

Furthermore, we have investigated the cycling performance of Mn<sub>2</sub>O<sub>3</sub>/HHC nanocomposite anode at a current density of 100 mA g<sup>-1</sup>. Fig. 7a and b illustrates the cycling performance and charge-discharge voltage profile of Mn<sub>2</sub>O<sub>3</sub>/HHC nanocomposite anode in the voltage range of 0.01 to 3.0 V. As expected, Mn<sub>2</sub>O<sub>3</sub>/HHC nanocomposite anode shows excellent electrochemical performance in terms of capacity and reversibility under the influence of 100 mA g<sup>-1</sup> current density also. More interestingly, Mn<sub>2</sub>O<sub>3</sub>/HHC nanocomposite anode exhibits 79 % of its theoretical capacity (806 mAh g<sup>-1</sup>) at 100 mA g<sup>-1</sup>, even after the completion of 200 cycles. Again, to our knowledge, this is the highest value reported so far in the literature (Table 1).<sup>20-30</sup>

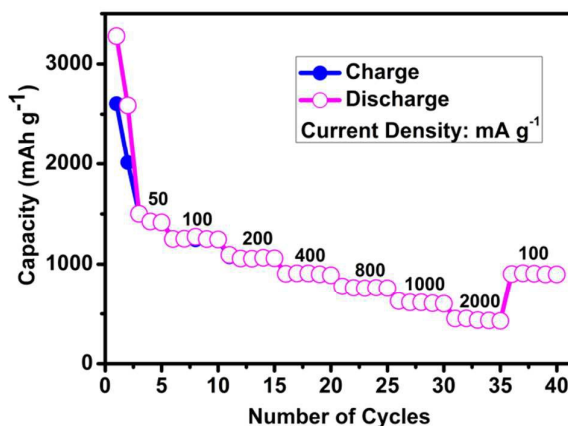


Fig. 8 Rate capability of Mn<sub>2</sub>O<sub>3</sub>/HHC nanocomposite anode under the influence of different current density values

To investigate the rate capability, Mn<sub>2</sub>O<sub>3</sub>/HHC nanocomposite anode was subjected to a range of current density varying from 50 to 2000 mA g<sup>-1</sup> and the effect of each current density was studied for every subsequent 5 cycles under the mode of continuous charge-discharge process. The outstanding rate capability behavior of Mn<sub>2</sub>O<sub>3</sub>/HHC nanocomposite anode is demonstrated by the specific discharge capacities observed around 1415, 1250, 1060, 890, 760, 600 and 440 mAh g<sup>-1</sup> at current densities such as 50, 100, 200, 400, 800, 1000 and 2000 mA g<sup>-1</sup> respectively (Fig. 8). As expected, the discharge capacity gradually decreased with the increasing current density. Even at a high current density of 2 A g<sup>-1</sup> (2C), the large reversible capacity of 440 mAh g<sup>-1</sup> is obtained. After cycling at various high current densities, the current density was brought back to 100 mA g<sup>-1</sup> and the specific capacity that could be recovered is found to be 890 mAh g<sup>-1</sup>, implying highly stable cycling performance and excellent reversibility of Mn<sub>2</sub>O<sub>3</sub>/HHC anode. The currently observed rated capacity is also two times higher than the theoretical capacity of commercial graphite (372 mAh g<sup>-1</sup>). To the best of our knowledge, this is the highest capacity that has been reported so far for Mn<sub>2</sub>O<sub>3</sub> based anode materials at higher current rates (Table 1).<sup>20-30</sup> The unique nanostructure of

Mn<sub>2</sub>O<sub>3</sub> and its complete wrapping with the randomly oriented graphene sheet like structure of HHC effectively shortens the lithium diffusion length, providing faster mass transfer with the effective alleviation of severe volume change effects. The synergistic effect of the above said advantages of Mn<sub>2</sub>O<sub>3</sub>/HHC nanocomposite anode thus favors the long term cycling and significantly enhances the lithium storage performance at high rates.<sup>31-34,36,38,39</sup>

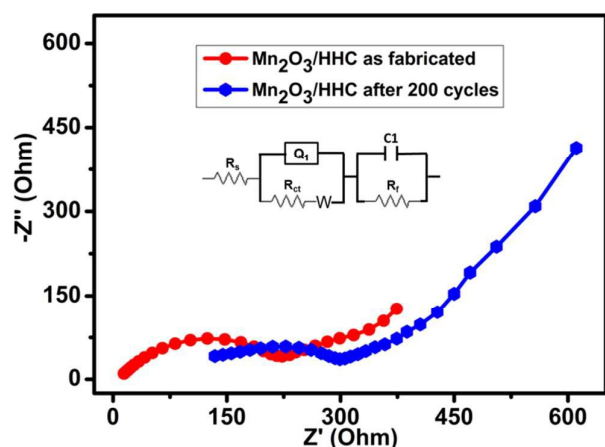


Fig. 9 Electrochemical impedance spectroscopy of  $\text{Mn}_2\text{O}_3/\text{HHC}$  nanocomposite anode

The  $\text{Mn}_2\text{O}_3/\text{HHC}$  nanocomposite anode exhibits low charge transfer resistance ( $R_{ct}$  ~220  $\Omega$ ) and high lithium-ion diffusion even after 200 cycles. There is no obvious change in the  $R_{ct}$  (270  $\Omega$ ) value of  $\text{Mn}_2\text{O}_3/\text{HHC}$  nanocomposite anode after 200 cycles compared with that of the as prepared cell (270  $\Omega$ ). This result once again confirms that the interconnected HHC layers increase the conductivity of the composite electrode and offer the required long term cycle life benefit also.<sup>31-39</sup>

Based on the discussed electrochemical properties,  $\text{Mn}_2\text{O}_3/\text{HHC}$  nanocomposite could be considered as a promising electrode material for application in LIBs. The below mentioned multiple synergistic effect of the  $\text{Mn}_2\text{O}_3/\text{HHC}$  nanocomposite anode is believed to be responsible for the extraordinarily high and stable energy storage performance.

- I. The complete wrapping of  $\text{Mn}_2\text{O}_3$  nanoparticles by the N and S containing porous sheets of HHC provides an efficient electrical conductivity to facilitate the easy and fast charge transfer.
- II. HHC sheets offer a spare space to accommodate the huge volume change experienced by  $\text{Mn}_2\text{O}_3$  nanoparticles during cycling process. In addition, the presence  $\text{Mn}_2\text{O}_3$  particles in nano size can shorten the diffusion length of the lithium-ions and favour the fast accessibility.
- III. Presence of hetero atoms in HHC can enhance the electrochemical performance by increasing the chemical reactivity, defect sites and electronic conductivity.

## Conclusion

In summary, we propose a new nanocomposite formulation, where  $\text{Mn}_2\text{O}_3$  nanoparticles wrapped in N and S containing randomly oriented graphene sheet like carbon (HHC) could be produced through a simple, scalable and facile method. Excellent electrochemical performance in terms of capacity,

long cycle life and rate capability has been achieved for the thus prepared  $\text{Mn}_2\text{O}_3/\text{HHC}$  nanocomposite, which is superior than any other  $\text{Mn}_2\text{O}_3$  anode materials reported so far. Interestingly, the key problems associated with pristine  $\text{Mn}_2\text{O}_3$  anode material, such as inferior conductivity and severe volume change have been mitigated to a greater extent due to the addition of HHC, which is a cheap and eco-benign composite additive, obtained from bio-waste (human hair). A reversible lithium storage capacity of 990  $\text{mAh g}^{-1}$  over 350 cycles at 50  $\text{mA g}^{-1}$  and 440  $\text{mAh g}^{-1}$  at 2000  $\text{mA g}^{-1}$  (2C) have been exhibited by  $\text{Mn}_2\text{O}_3/\text{HHC}$  anode, which is the highest value reported for  $\text{Mn}_2\text{O}_3$  anode in the literature. Hence, it is hereby recommended that  $\text{Mn}_2\text{O}_3/\text{HHC}$  nanocomposite anode could be considered as a promising candidate for next generation energy storage applications.

## Acknowledgements

Financial support from University Grants Commission for the UGC- Senior Research Fellowship and Council of Scientific and Industrial Research (CSIR) through MULTIFUN program is gratefully acknowledged.

## References

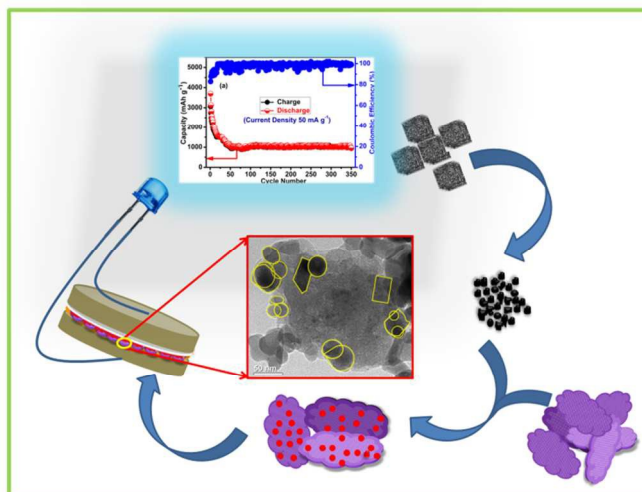
- 1 B. Dunn, H. Kamath and J. M. Tarascon, *Science*, 2011, **334**, 928.
- 2 J. M. Tarascon and M. Armand, *Nature*, 2001, **414**, 359.
- 3 S. Nam, S. Kim, S. Wi, H. Choi, S. Byun, S. Choi, S. Yoo, K. T. Lee and B. Park, *J. Power Sources*, 2012, **211**, 154.
- 4 P. Wu, N. Du, H. Zhang, J. Yu, Y. Qi and D. Yang, *Nanoscale*, 2011, **3**, 746.
- 5 N. Yan, L. Hu, Y. Li, Y. Wang, H. Zhong, X. Hu, X. Kong and Q. Chen, *J. Phys. Chem. C*, 2012, **116**, 7227.
- 6 B. Zhang, Q. B. Zheng, Z. D. Huang, S. W. Oh and J. K. Kim, *Carbon*, 2011, **49**, 4524.
- 7 Z. S. Wu, W. C. Ren, L. Wen, L. B. Gao, J. P. Zhao, Z. P. Chen, G. M. Zhou, F. Li and H. M. Cheng, *ACS Nano*, 2010, **4**, 3187.
- 8 L. Fei, Q. Lin, B. Yuan, M. Naeemi, Y. Xu, Y. Li, S. Deng and H. Luo, *Mater. Lett.*, 2013, **98**, 59.
- 9 Y. F. Deng, Z. N. Li, Z. C. Shi, H. Xu, F. Peng and G. H. Chen, *RSC Adv.*, 2012, **2**, 4645.
- 10 X. M. Yin, L. B. Chen, C. C. Li, Q. Y. Hao, S. Liu, Q. H. Li, E. D. Zhang and T. H. Wang, *Electrochim. Acta*, 2011, **56**, 2358.
- 11 J. S. Chen, L. A. Archer and X. W. Lou, *J. Mater. Chem.*, 2011, **21**, 9912.
- 12 F. Zhang, Y. Zhang, S. Y. Song and H. J. Zhang, *J. Power Sources*, 2011, **196**, 8618.
- 13 Y. Sun, X. Y. Feng and C. H. Chen, *J. Power Sources*, 2011, **196**, 784.
- 14 K. T. Nam, D. W. Kim, P. J. Yoo, C. Y. Chiang, N. Meethong, P. T. Hammond, Y. M. Chiang and A. M. Belcher, *Science*, 2006, **312**, 885.
- 15 Y. Lu, Y. Wang, Y. Q. Zou, Z. Jiao, B. Zhao, Y. Q. He and M. H. Wu, *Electrochem. Commun.*, 2010, **12**, 101.
- 16 S. Vijayanand, R. Kannan, H. S. Potdar, V. K. Pillai and P. A. Joy, *J. Appl. Electrochem.*, 2013, **43**, 995.
- 17 L. Pan, L. Li and Q. Y. Zhu, *J. Sol.-Gel. Sci. Technol.*, 2013, **67**, 573.
- 18 D. Q. Liu, X. Wang, X. B. Wang, W. Tian, Y. Bando and D. Golberg, *Sci. Rep.*, 2013, **3**, 2543.
- 19 J. Xu, L. Gao, J. Y. Cao, W. C. Wang and Z. D. Chen, *Electrochim. Acta*, 2010, **56**, 732.

- 20 H. B. Lin, H. B. Rong, W. Z. Huang, Y. H. Liao, L. D. Xing, M. Q. Xu, X. P. Li and W. S. Li, *J. Mater. Chem. A*, 2014, **2**, 14189.
- 21 Q. Li, L. Yin, Z. Li, X. Wang, Y. Qi and J. Ma, *ACS Appl. Mater. Interfaces*, 2013, **5**, 10975.
- 22 X. Zhang, Y. Qian, Y. Zhu and K. Tang, *Nanoscale*, 2014, **6**, 1725.
- 23 Y. Qiao, Y. Yua, Y. Jin, Y. –B. Guan and C. –H. Chena, *Electrochim. Acta*, 2014, **132**, 323.
- 24 Y. Deng, Z. Li, Z. Shi, H. Xu, F. Peng and G. Chen, *RSC Adv.*, 2012, **2**, 4645.
- 25 L. Chang, L. Mai, X. Xu, Q. An, Y. Zhao, D. Wanga and X. Feng, *RSC Adv.*, 2013, **3**, 1947.
- 26 Y. Dai, H. Jiang, Y. Hu and C. Li, *RSC Adv.*, 2013, **3**, 19778.
- 27 Y. Qiu, G. –L. Xu, K. Yan, H. Sun, J. Xiao, S. Yang, S. –g. Sun, L. Jind and H. Deng, *J. Mater. Chem.*, 2011, **21**, 6346.
- 28 H. Su, Y. –F. Xu, S. –C. Feng, Z. –G. Wu, X. –P. Sun, C. –H. Shen, J. –Q. Wang, J. –T. Li, L. Huang and S. –G. Sun, *ACS Appl. Mater. Interfaces*, 2015, **7**, 8488.
- 29 Y. Zhang, Y. Yan, X. Wang, G. Li, D. Deng, L. Jiang, C. Shu and C. Wang, *Chem. Eur. J.*, 2014, **20**, 6126.
- 30 Y. Sun, L. Hu, F. Zhang and Q. Chen, *J. Alloys and Compounds*, 2013, **576**, 86.
- 31 Y. Gu, Y. Xu and Y. Wang, *ACS Appl. Mater. Interfaces*, 2013, **5**, 801.
- 32 Y. Huang, X. L. Huang, J. S. Lian, D. Xu, L. M. Wang and X. B. Zhang, *J. Mater. Chem.*, 2012, **22**, 2844.
- 33 C. T. Hsieh, J. S. Lin, Y. F. Chen and H. Teng, *J. Phys. Chem. C*, 2012, **116**, 15251.
- 34 C. Xu, J. Sun and L. Gao, *Nanoscale*, 2012, **4**, 5425.
- 35 K. Chang and W. Chen, *ACS Nano*, 2011, **5**, 4720.
- 36 KR. Saravanan and N. Kalaiselvi, *Carbon*, 2014, **81**, 43.
- 37 B. Chandra sekhar, Ganguli Babu and N. Kalaiselvi. *RSC Adv.*, 2015, **5**, 4568.
- 38 L. Fei, Q. Lin, B. Yuan, G. Chen, P. Xie, Y. Li, Y. Xu, S. Deng, S. Smirnov and H. Luo, *ACS Appl. Mater. Interfaces*, 2013, **5**, 5330.
- 39 J. Hou, C. Cao, F. Idrees and X. Ma, *ACS Nano*, 2015, **9**, 2556.

**Validation of Green Composite Containing Nanocrystalline  $\text{Mn}_2\text{O}_3$  and Biocarbon  
Derived from Human Hair as a Potential Anode for Lithium-ion Batteries**

*Chandra Sekhar Bongu, Saravanan Karuppiah and Kalaiselvi Nallathamby\**

**Graphical Abstract:**



A newer formulation of green composite of nanocrystalline  $\text{Mn}_2\text{O}_3$ , viz.,  $\text{Mn}_2\text{O}_3/\text{HHC}$  containing biocarbon derived from human hair has been exploited for the first time as an anode that demonstrates superior capacity and rate capability in lithium-ion batteries.